Geophysical Research Letters

RESEARCH LETTER
10.1029/2025GL116561

Electromagnetic Ion Cyclotron Waves in a Magnetic Reconnection Exhaust at Earth's Magnetopause

Zewen Chen[1,2,3], Zhenpeng Su[1,2,3,4], Zhiyong Wu[1,2,3], Lei Dai[5], Tianran Sun[5], Binbin Tang[5], San Lu[1,2,3], Zhaoguo He[4], Huinan Zheng[1,2,3], and Yuming Wang[1,2,3]

[1]National Key Laboratory of Deep Space Exploration/School of Earth and Space Sciences, University of Science and Technology of China, Hefei, China, [2]CAS Center for Excellence in Comparative Planetology/CAS Key Laboratory of Geospace Environment/Mengcheng National Geophysical Observatory, University of Science and Technology of China, Hefei, China, [3]Collaborative Innovation Center of Astronautical Science and Technology, Harbin, China, [4]State Key Laboratory of Lunar and Planetary Sciences, Macau University of Science and Technology, Macau, China, [5]State Key Laboratory of Space Weather, National Space Science Center, Chinese Academy of Sciences, Beijing, China

Abstract Plasma waves can initiate, regulate, or reflect magnetic reconnection efficiently converting magnetic energy into plasma energy. While waves ranging from below the ion cyclotron frequency to above the electron plasma frequency are commonly observed near reconnection sites, electromagnetic ion cyclotron (EMIC) waves—frequent in other plasma environments—have been rarely observed in the reconnection region. Here, we report the first detection of EMIC waves in a magnetic reconnection exhaust at Earth's magnetopause. The free energy required for EMIC wave growth was supplied by the strong perpendicular-to-parallel temperature anisotropy of hot proton beams. This proton temperature anisotropy was generated by magnetopause reconnection, rather than inherited from the magnetosheath. Our findings differ from previous reports of parallel-preferential proton heating during magnetopause reconnection, calling for revised theoretical frameworks to reconcile observed perpendicular-preferential heating with established reconnection paradigms.

Plain Language Summary Magnetic reconnection is a fundamental process responsible for explosive energy releases in events such as geomagnetic storms, solar flares, and astrophysical jets. Plasma waves play crucial roles as triggers, regulators, or indicators of magnetic reconnection activities. While various types of waves have been observed near reconnection sites, one common type—the electromagnetic ion cyclotron (EMIC) wave—had been rarely observed in reconnection region until now. We have discovered these previously missing EMIC waves at Earth's magnetopause, the boundary where the solar wind impinges on Earth's magnetic field. These waves were excited by hot protons that had been heated more strongly perpendicular to the magnetic field lines than along them. This finding contradicts decades of research suggesting that hot protons should primarily be heated along the magnetic field lines during the magnetopause reconnection. It challenges our current understanding of how energy is distributed during collisionless reconnection, highlighting the need for revised theoretical models to explain the observed perpendicular-preferential heating.

Key Points:

- Electromagnetic ion cyclotron waves were observed in a magnetic reconnection exhaust at Earth's magnetopause
- Hot proton beams with perpendicular-to-parallel temperature anisotropies provided free energy necessary for the excitation of these waves
- Ion heating in the magnetic reconnection exhaust exhibited a clear perpendicular preference, unlike previous reports

Supporting Information:

Supporting Information may be found in the online version of this article.

Correspondence to:

Z. Su and Z. He,
szpe@mail.ustc.edu.cn;
zghe@must.edu.mo

Citation:

Chen, Z., Su, Z., Wu, Z., Dai, L., Sun, T., Tang, B., et al. (2025). Electromagnetic ion cyclotron waves in a magnetic reconnection exhaust at Earth's magnetopause. *Geophysical Research Letters*, *52*, e2025GL116561. https://doi.org/10.1029/2025GL116561

Received 16 APR 2025
Accepted 15 SEP 2025

1. Introduction

Magnetic reconnection is a universal process that converts magnetic energy into plasma energy across experimental, space, and astrophysical plasma environments (e.g., Burch et al., 2016; Dai et al., 2024; Lee & Lee, 2020; Parker, 1957). Plasma waves are prevalent in nearly all regions associated with the reconnection process (see review by M. Fujimoto et al., 2011; Khotyaintsev et al., 2019; Vaivads et al., 2006; Zhou et al., 2022). Pre-existing waves can initiate magnetic reconnection (e.g., Deng & Matsumoto, 2001), while newly generated waves not only mirror the developmental characteristics of magnetic reconnection (M. Fujimoto et al., 2011) but also influence its progression by modifying particle distributions (e.g., Drake et al., 2003).

A wide spectrum of waves, ranging from below the ion cyclotron frequency to above the electron plasma frequency, has been observed near reconnection sites. Electromagnetic radio emission above the electron plasma frequency is thought to generate from reconnection sites (Sakai et al., 2005), allowing remote diagnostics of reconnection events in the solar corona (Bastian et al., 1998). Upper hybrid waves can be excited by agyrotropic electron distributions (B. B. Tang et al., 2019) in the separatrix region (Farrell et al., 2002) and electron diffusion region (Graham et al., 2017). Similarly, electron Bernstein waves can be driven by crescent-shaped electron

distributions in the separatrix region (Graham et al., 2018) and electron diffusion region (Li et al., 2020). Langmuir waves have been identified in the separatrix region (Deng et al., 2004) and electron diffusion region (Burch et al., 2019), as confirmed by particle-in-cell simulations (K. Fujimoto, 2014; Pritchett & Coroniti, 2004). Electrostatic waves have been reported across multiple regions: outflow region (Matsumoto et al., 2003), separatrix region (Cattell et al., 2005; Retinò et al., 2006), and electron diffusion region (Yu et al., 2021), with their presence further validated by particle-in-cell simulations (Chang et al., 2021, 2022; K. Fujimoto, 2014; K. Fujimoto & Machida, 2006; Lapenta et al., 2011). Observational evidence supports a link between electrostatic solitary waves and electron phase space holes (Drake et al., 2003; Mozer et al., 2018). Whistler-mode waves generated by electrons heated adiabatically downstream of the reconnection jet and within the separatrix region were predicted by particle-in-cell simulations (K. Fujimoto, 2014; K. Fujimoto & Sydora, 2008; Goldman et al., 2014). Evidence for whistler-mode waves has accumulated in the flux pileup region at the front of reconnection jets (Fu et al., 2014; Khotyaintsev et al., 2011), in the separatrix region (Huang et al., 2016; Ren et al., 2019), in the ion diffusion region (Fu et al., 2019), and in the electron diffusion region (Ren et al., 2024; X. Tang et al., 2013). Lower hybrid waves have been detected in the dipolarization front of reconnection jets (Divin, Khotyaintsev, Vaivads, & André, 2015; Zhou et al., 2009), separatrix region (Ren, Dai, Wang, & Guo, 2023; Ren, Dai, Wang, & Lavraud, 2023; Ren et al., 2022; Retinò et al., 2006), and ion diffusion region (Bale et al., 2002), with supporting results from particle-in-cell simulations (Roytershteyn et al., 2012, 2013) as well as kinetic modeling (Divin, Khotyaintsev, Vaivads, André, Markidis, & Lapenta, 2015). Lower hybrid waves are thought to provide anomalous resistivity in the diffusion region (Daughton, 2003; K. Fujimoto & Sydora, 2012). Kinetic Alfvén waves play a crucial role in forming the Hall electromagnetic structure in the diffusion region (Dai, 2009; Dai et al., 2017; Duan et al., 2017; Huang et al., 2010; Rogers et al., 2001). Despite the diversity of these waves, one common wave in plasma physics—the electromagnetic ion cyclotron (EMIC) wave—has notably been absent from this spectrum.

In this Letter, we report, for the first time, the observation of EMIC waves within a magnetic reconnection exhaust at Earth's magnetopause. These waves are generated by anisotropic hot proton beams that experience significant perpendicular heating as they flow from the magnetosheath into reconnection jet. This finding shows new heating features that are different from previous theoretical and observational studies (Drake, Cassak, et al., 2009; Drake, Swisdak, et al., 2009; Hoshino et al., 1997; Phan et al., 2014; Wang et al., 2023; Wu et al., 2013), which typically suggest parallel-preferential heating during magnetopause reconnection. The conditions and mechanisms responsible for the observed perpendicular-preferential heating of protons during magnetopause reconnection would be highly interesting for understanding energy conversion of reconnection.

2. Data and Method

We here use the observations made by the probe A (TH-A) of the Time History of Events and Macroscales Interactions during Substorms (THEMIS) mission (Angelopoulos, 2008). The ElectroStatic Analyzer (ESA) measured the three-dimensional velocity distributions of ions and electrons with a time resolution of $\sim$3 s (McFadden et al., 2008). The flux Magnetometer (FGM) (Auster et al., 2008) measured the magnetic field vectors of a 128 Hz sampling rate. The Electric field instrument (EFI) (Bonnell et al., 2008) measured the electric field vectors of a 8 Hz sampling rate in the spin plane, while the component along the spin axis was derived using the condition $\mathbf{E}\cdot\mathbf{B} = 0$.

To analyze the configuration of magnetopause reconnection, we apply the minimum variance analysis (MVA) technique (Sonnerup & Cahill, 1967) to the FGM measurements. In the resulting magnetopause-MVA coordinate system, **L**, **M**, and **N** represent the maximum, intermediate, and minimum variance directions, respectively. Both the reconnecting magnetic component and the reconnection jet approximately align with **L**. To understand the propagation characteristics of waves, we introduce a mean-field-aligned (MFA) coordinate system. In this system, $\mathbf{e}_{\parallel}$ is defined along the 8 s running average of the FGM measurements, $\mathbf{e}_{\perp 1}$ lies in the direction of the cross product of $\mathbf{e}_{\parallel}$ and the ion bulk velocity, and $\mathbf{e}_{\perp 2} = \mathbf{e}_{\perp 1} \times \mathbf{e}_{\parallel}$ completes the orthogonal triad. Wave analysis proceeds through the following steps: (a) applying a 0.25 Hz high-pass filter to isolate the EMIC wave frequency band from FGM measurements; (b) computing electromagnetic power spectral density matrices using Fast Fourier Transform; (c) deriving the Poynting flux vector from cross-power spectral densities (Santolík et al., 2010); and (d) estimating the wave normal angle, polarization, and planarity using the singular value decomposition technique (Santolík et al., 2002, 2003).

We model the observed ion phase space density (PSD) as a superposition of multiple κ-Maxwellian distributions (Hellberg & Mace, 2002; Sugiyama et al., 2015) with the same perpendicular drift velocity (i.e., the ion perpendicular bulk velocity $v_{\perp \mathrm{d}}$) but different parallel drift velocities. In the MFA coordinate system, the ion PSD can be expressed as

$$F\left(v_{\parallel}, v_{\perp 1}, v_{\perp 2}\right)=\sum_{s=1}^{N} F_{\kappa \mathrm{M},s}\left(v_{\parallel}, v_{\perp 1}, v_{\perp 2}\right), \tag{1}$$

$$F_{\kappa \mathrm{M},s}\left(v_{\parallel}, v_{\perp 1}, v_{\perp 2}\right)=n_s f_{\kappa,s}\left(v_{\parallel}\right) f_{\mathrm{M}_1,s}\left(v_{\perp 1}\right) f_{\mathrm{M}_2,s}\left(v_{\perp 2}\right), \tag{2}$$

$$f_{\kappa,s}\left(v_{\parallel}\right)=\frac{1}{\sqrt{\pi}\theta_{\parallel s}} \frac{\Gamma\left(\kappa_s\right)}{\sqrt{\kappa_s}\Gamma\left(\kappa_s-1/2\right)}\left[1+\frac{\left(v_{\parallel}-v_{\parallel \mathrm{d}s}\right)^2}{\kappa_s \theta_{\parallel s}^2}\right]^{-\kappa_s}, \tag{3}$$

$$f_{\mathrm{M}_1,s}\left(v_{\perp 1}\right)=\frac{1}{\sqrt{\pi}\theta_{\perp s}} \exp\left[-\frac{v_{\perp 1}^2}{\theta_{\perp s}^2}\right], \tag{4}$$

$$f_{\mathrm{M}_2,s}\left(v_{\perp 2}\right)=\frac{1}{\sqrt{\pi}\theta_{\perp s}} \exp\left[-\frac{\left(v_{\perp 2}-v_{\perp \mathrm{d}}\right)^2}{\theta_{\perp s}^2}\right], \tag{5}$$

where the subscript s refers to the sth component with density n_s, parallel drift velocity $v_{\parallel \mathrm{d}s}$, parallel thermal velocity $\theta_{\parallel s}=\sqrt{\left(2-3/\kappa_s\right) k_{\mathrm{B}} T_{\parallel s}/m_{\mathrm{i}}}$, perpendicular thermal velocity $\theta_{\perp s}=\sqrt{2 k_{\mathrm{B}} T_{\perp s}/m_{\mathrm{i}}}$, parallel temperature $T_{\parallel s}$, perpendicular temperature $T_{\perp s}$, and Kappa parameter κ_s, m_{i} is the proton mass, k_{B} is the Boltzmann constant, and Γ is the Gamma function. In a reference frame moving with velocity $v_{\perp \mathrm{d}}$ along the $\mathbf{e}_{\perp 2}$ direction, we utilize the BO-KM code (Bai et al., 2025; Xie, 2019) to evaluate the linear instability of ions. For waves propagating parallel or antiparallel to the background magnetic field, the wave frequency remains unchanged between the BO-KM reference frame and the satellite reference frame.

3. Event Overview

From 16:53:00 UT to 16:56:00 UT on 7 June 2014 (Figure 1), TH-A traversed from the magnetosphere through the boundary layer into the magnetosheath near the dawnside equatorial region (R = 10.39, MLT = 8.16, MLAT = 7.12). Prior to 16:53:36 UT, TH-A sampled the magnetosphere, characterized by a relatively stable magnetic field (Figure 1e), low plasma density ($\sim$ <1 cm^{-3} in Figure 1a), and the presence of energetic ions (>5 keV in Figure 1b) and electrons (>1 keV in Figure 1c). In contrast, after 16:54:10 UT, TH-A sampled the magnetosheath, characterized by a fluctuating magnetic field, high plasma density ($\sim$ >20 cm^{-3}), and the presence of suprathermal ions (0.1–5.0 keV) and electrons (0.01–0.5 keV). Between them was the boundary layer with a mixture of magnetospheric and magnetosheath plasma (Hasegawa, 2012). Within the boundary layer, the energetic electrons (3–30 keV) exhibited one-sided pitch-angle distributions (Figure 1d), suggesting the reconnection of terrestrial and interplanetary magnetic field lines (Gosling et al., 1990; Paschmann et al., 1979). Another signature of the magnetopause reconnection was the presence of high-speed ion jet within the boundary layer. In the Sweet-Parker-type asymmetric reconnection framework (Cassak & Shay, 2007; Walsh et al., 2014), the outflow ions are accelerated to the hybrid Alfvén speed

$$V_{\mathrm{A}}=\sqrt{\frac{B_{\mathrm{L,mp}} B_{\mathrm{L,ms}}\left(B_{\mathrm{L,mp}}+B_{\mathrm{L,ms}}\right)}{\mu_0\left(\rho_{\mathrm{mp}} B_{\mathrm{L,ms}}+\rho_{\mathrm{ms}} B_{\mathrm{L,mp}}\right)}}, \tag{6}$$

where the subscript mp and ms respectively represent the parameters in the magnetosphere and magnetosheath, B_{L} is the reconnecting magnetic component, ρ is ion mass density, and μ_0 is vacuum permeability. Averaging measurements in the magnetosphere from 16:53:25 UT to 16:53:35 UT gives $B_{\mathrm{L,mp}}$ = 54.6 nT and ρ_{mp} = 2.1 $\times$ 10^{-21} kg $\cdot$ m^{-3}, and averaging measurements in the magnetosheath from 16:54:10 UT to 16:54:20 UT gives $B_{\mathrm{L,ms}}$ = 31.3 nT and ρ_{ms} = 5.5 $\times$ 10^{-20} kg $\cdot$ m^{-3}. Given these parameters, we obtain the hybrid

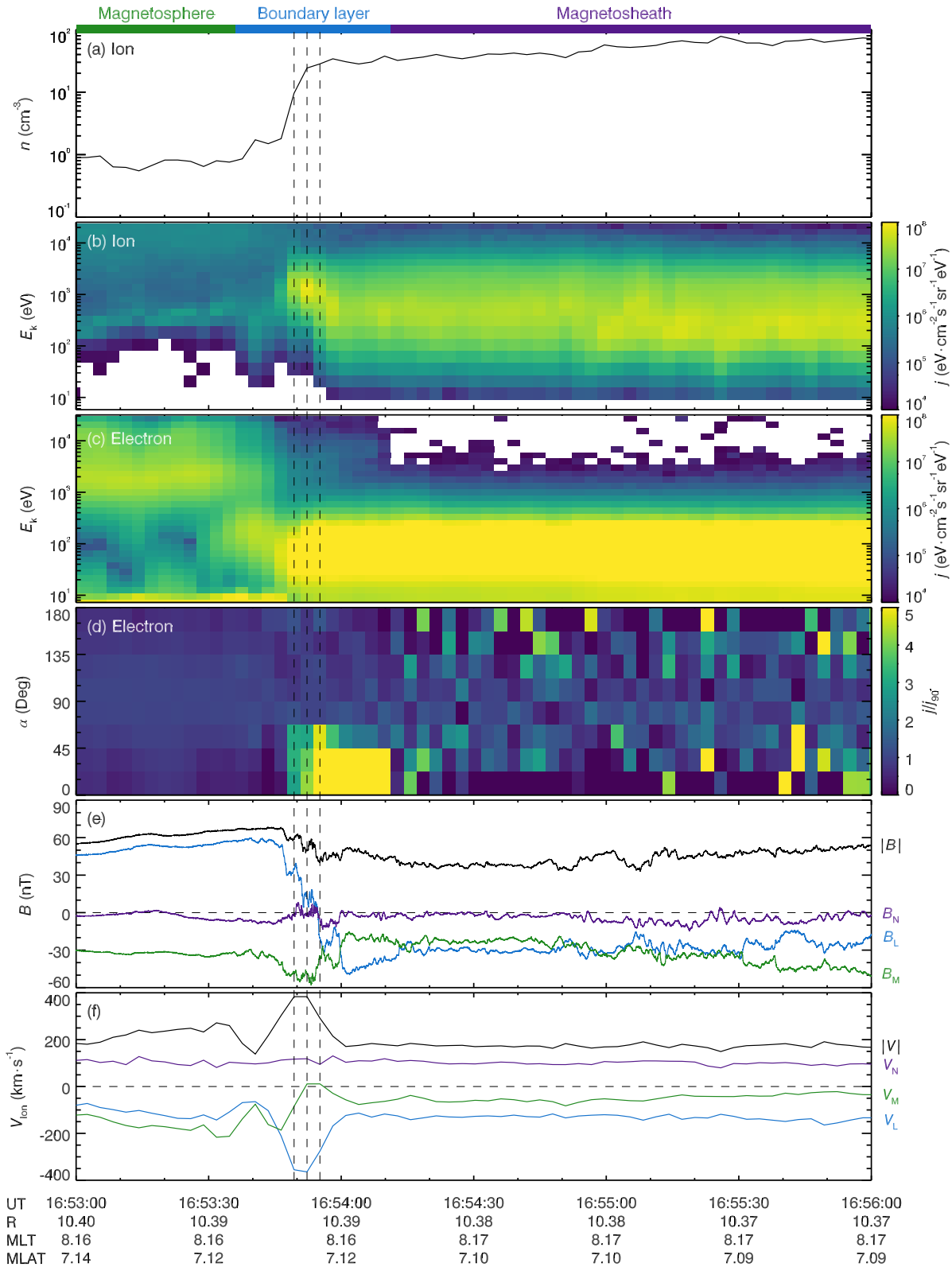

Figure 1.

Alfvén speed $V_A = 196.3\ \mathrm{km \cdot s^{-1}}$. The observed ion jet velocity relative to the magnetosheath flow was $V_{jet} = V_{L,max} - V_{L,ms} = 220.3\ \mathrm{km \cdot s^{-1}}$, generally consistent with the theoretical prediction.

In the magnetosheath (16:54:10–16:56:00 UT), there were electromagnetic waves near the proton cyclotron frequency exhibiting left-handed polarization and field-aligned propagation (Figure 2). These waves were the well-known EMIC waves (Anderson et al., 1994; Denton et al., 1994; Remya et al., 2014; Zhao et al., 2019), which were probably generated by anisotropic protons with a higher perpendicular temperature $(T_\perp)$ than parallel temperature $(T_\parallel)$ (Gary, 1992; Gary et al., 1993). The most striking phenomenon was the occurrence of similar waves in the boundary layer (16:53:41–16:54:10 UT). Particularly within the magnetic reconnection exhaust region (corresponding to the reconnection jet around 16:53:52 UT), the intense waves displayed frequency chirping characteristics similar to those of EMIC waves commonly observed in the inner magnetosphere (Grison et al., 2018; Nakamura et al., 2016; Omura et al., 2010; Pickett et al., 2010). Rising-tone waves exhibited right-handed polarization and propagated from northward regions toward the spacecraft, roughly aligning with the reconnection jet direction (Figure 2a). Falling-tone waves showed left-handed polarization, though their propagation characteristics remained unresolved due to data gaps (Figure 2d). The superposition of these oppositely polarized modes impeded robust estimation of wave normal angles, resulting in broad angular scattering (Figure 1e). The observed wave characteristics in the magnetic reconnection exhaust were inconsistent with those of lower-hybrid waves, which typically exhibit quasi-perpendicular propagation and nearly linear polarization (Graham et al., 2019; Roytershteyn et al., 2012). Instead, these features were robustly consistent with those of EMIC waves, which can have peak growth rates at the field-aligned propagation angles and support both left- and right-handed polarizations (Gary, 1991).

4. EMIC Wave Generation Within the Magnetic Reconnection Exhaust

The first column of Figure 3 displays the observed and modeled ion velocity distributions on the $\mathbf{e}_\parallel$–$\mathbf{e}_{\perp 2}$ plane at three adjacent time moments within the magnetic reconnection exhaust. There were significant spatial and temporal variations in the ion velocity distributions within the reconnection exhaust. A superposition of two κ-Maxwellian components is able to adequately reproduce the observed distribution at each moment. As listed in Table S1 in Supporting Information S1, each ion component exhibited a strong temperature anisotropy with $A = T_\perp/T_\parallel - 1$ ranging from 1.5 to 3.1, representing a twofold variation during the 9-s observation window. Meanwhile, the parallel drift velocity exhibited sign reversal in the MFA coordinate system due to local magnetic field reversal. These multiple anisotropic and drifting plasma components produce dispersion relations that substantially differ from those of cold or static plasma predictions (Davidson & Ogden, 1975; Horne & Thorne, 1993). One of the most obvious features in the proton beam system is that left- and right-handed polarized waves can extend in frequency from below to above the proton gyrofrequency (e.g., Zhao et al., 2019). The observed large temperature anisotropies, combined with small relative parallel drift velocities between the two proton components, strongly favor wave excitation via proton temperature anisotropy instability over beam instability. The magnetic field direction at 16:53:49 UT and 16:53:52 UT was approximately opposite to that at 16:53:55 UT (Figure 2a). The wave propagation from northward regions toward the spacecraft corresponds to anti-parallel propagation ($\omega/k < 0$) at the first two time moments, but to parallel propagation ($\omega/k > 0$) at the third time moment.

The remaining three columns of Figure 3 present results from various linear instability tests under different assumptions. The second column represents a baseline scenario using the locally observed magnetic field strength, corresponding to in situ wave generation. In the third column, motivated by two physical considerations: (a) wave generation may preferentially occur where the magnetic field is weakest along the field line (Horne & Miyoshi, 2016; Keika et al., 2012; McCollough et al., 2010; Vines et al., 2019), and (b) near the reconnection site, the magnetic field intensity could also be relatively low, we accordingly reduce the magnetic field strength to 25 nT. This 25 nT value, ~50% of near-equatorially measured values, approximately matches the predicted

Figure 1. A magnetopause crossing by TH-A from 16:53:00 UT to 16:56:00 UT on 7 June 2014. (a) Ion density. (b) Ion and (c) electron differential energy fluxes (color-coded). (d) Pitch-angle-dependent differential energy flux of 3,394–30,333 eV electrons (color-coded), normalized by its instantaneous value at the pitch angle of 90°. (e) Magnetic field and (f) ion velocity in the magnetopause-LMN coordinate system. Line colors help differentiate among the magnitude and three components. Colors in the top bar help differentiate the magnetosphere (green), the boundary layer (blue), and the magnetosheath (purple), respectively. The three vertical dashed lines mark key time moments (16:53:49 UT, 16:53:52 UT, and 16:53:55 UT) that are analyzed in detail in Figure 3.

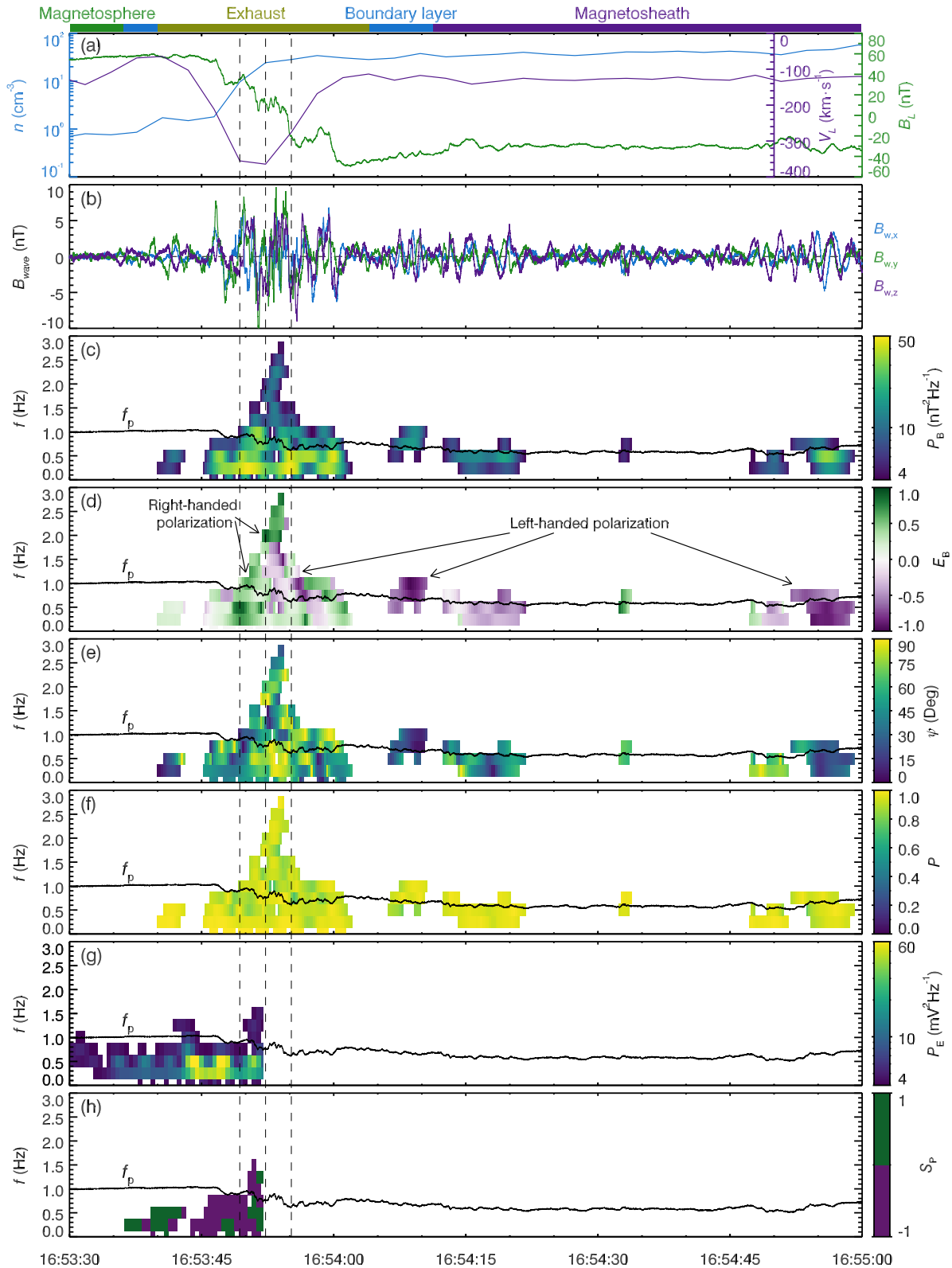

Figure 2.

minimum-field strength along the field line (Tsyganenko & Sitnov, 2005). In the fourth column, motivated by observations of the upstream solar wind showing an α-to-proton density ratio ranging from 1.5% to 8.5% (Figure S4 in Supporting Information S1), we further include a 5% He^{++} component with the same parallel drift velocity as the second proton population and an isotropic temperature of 100 eV. These tests are not intended as comprehensive parameter surveys, but rather represent a set of purposefully selected scenarios aimed at revealing the fundamental physics of wave generation.

To reproduce the observed dominance of right-handed polarized waves propagating anti-parallel to the magnetic field, a reduced magnetic field strength is required at the first time moment, and the inclusion of He^{++} is additionally necessary at the second. These results support the interpretation that the wave source was located northward of the spacecraft, in a region of reduced magnetic field strength. At the third time moment, the dominance of parallel propagating, left-handed polarized waves is consistently observed across all tested configurations, showing relatively little sensitivity to variations in magnetic field strength or He^{++} abundance. In this case, the source location is less certain: it could be close to the spacecraft or still resided in the northern low-field region. Additional tests (Figures S1–S3 in Supporting Information S1), where the temperature anisotropy of each proton component is systematically enabled or disabled, identify which proton component dominates the excitation of each specific wave mode (Table S2 in Supporting Information S1). The complete cessation of wave generation when all proton temperature anisotropy is removed rules out significant wave growth via proton beam instability, which requires sufficiently large parallel drift velocities relative to the local Alfvén velocity between proton components (Gary, 1991).

Linear instability theory predicts wave growth at frequencies below $2f_p$, where f_p is the proton cyclotron frequency and scales with the local magnetic field strength. This predicted bandwidth is somewhat narrower than the observed wave activity. Additional nonlinear amplification processes (An et al., 2024; Omura et al., 2010; Tao et al., 2021) may account for the extended chirping structures observed in the data. Nonlinear wave growth typically occurs over broader frequency ranges and at significantly higher rates than predicted by linear theory (Omura et al., 2008, 2010, 2015). The observed frequency chirping may arise from phase space "hole" and "hill" structures formed through nonlinear phase trapping near the linear resonant velocity (Omura et al., 2015). Theoretical considerations suggest that abrupt variations in resonant velocity with frequency can disrupt this process, thereby limiting sustained chirping. Figure S5 in Supporting Information S1 demonstrates that the reconnection exhaust environment, unlike the inner magnetosphere (Omura et al., 2010; Pickett et al., 2010), permits smoother variation of EMIC wave resonant velocity with frequency, particularly at higher frequencies. This distinctive dispersion characteristic likely favors the extended frequency chirping range (normalized to f_p) observed in our reconnection exhaust measurements.

5. Discussion

Our analysis above is subject to several important limitations: (a) the restriction to linear instability theory, which does not account for nonlinear wave growth or evolution processes (An et al., 2024; Omura et al., 2010; Tao et al., 2021); (b) the inherent difficulty in precisely locating EMIC wave source regions from single-point measurements; (c) the approximation of source ion distributions by in situ measurements that may not fully capture the true source conditions; and (d) the instrumental inability to discriminate minor ion species. Despite these limitations, both our observations and theoretical calculations support the conclusion that proton temperature anisotropy provides the free energy necessary for EMIC wave growth within the magnetic reconnection exhaust. To the best of our knowledge, this study presents the first report of large-amplitude EMIC waves, exhibiting peak-to-peak magnetic field fluctuations up to 20 nT (Figure 2b), that are directly associated with magnetopause reconnection.

A natural question arises as to whether such proton temperature anisotropy was produced by magnetopause reconnection or derived from the magnetosheath. As shown in Table S1 and Figure S6 in Supporting

Figure 2. EMIC wave properties. (a) Ion density and velocity, and magnetic field. (b) >0.25 Hz magnetic signals of waves. (c) Magnetic power spectral density of waves. (d) Wave polarization (negative for left-handed polarization and positive for right-handed polarization). (e) Wave normal angle (with an inherent 180° uncertainty). (f) Planarity (with perfect plane waves corresponding to unity). (g) Electric power spectral density of waves. (h) Parallel Poynting flux sign (showing wave propagation direction relative to the background magnetic field). In the panels (c–h), the black curves indicate the local proton cyclotron frequency f_p. The three vertical dashed lines mark key time moments (16:53:49 UT, 16:53:52 UT, and 16:53:55 UT) that are analyzed in detail in Figure 3.

10.1029/2025GL116561

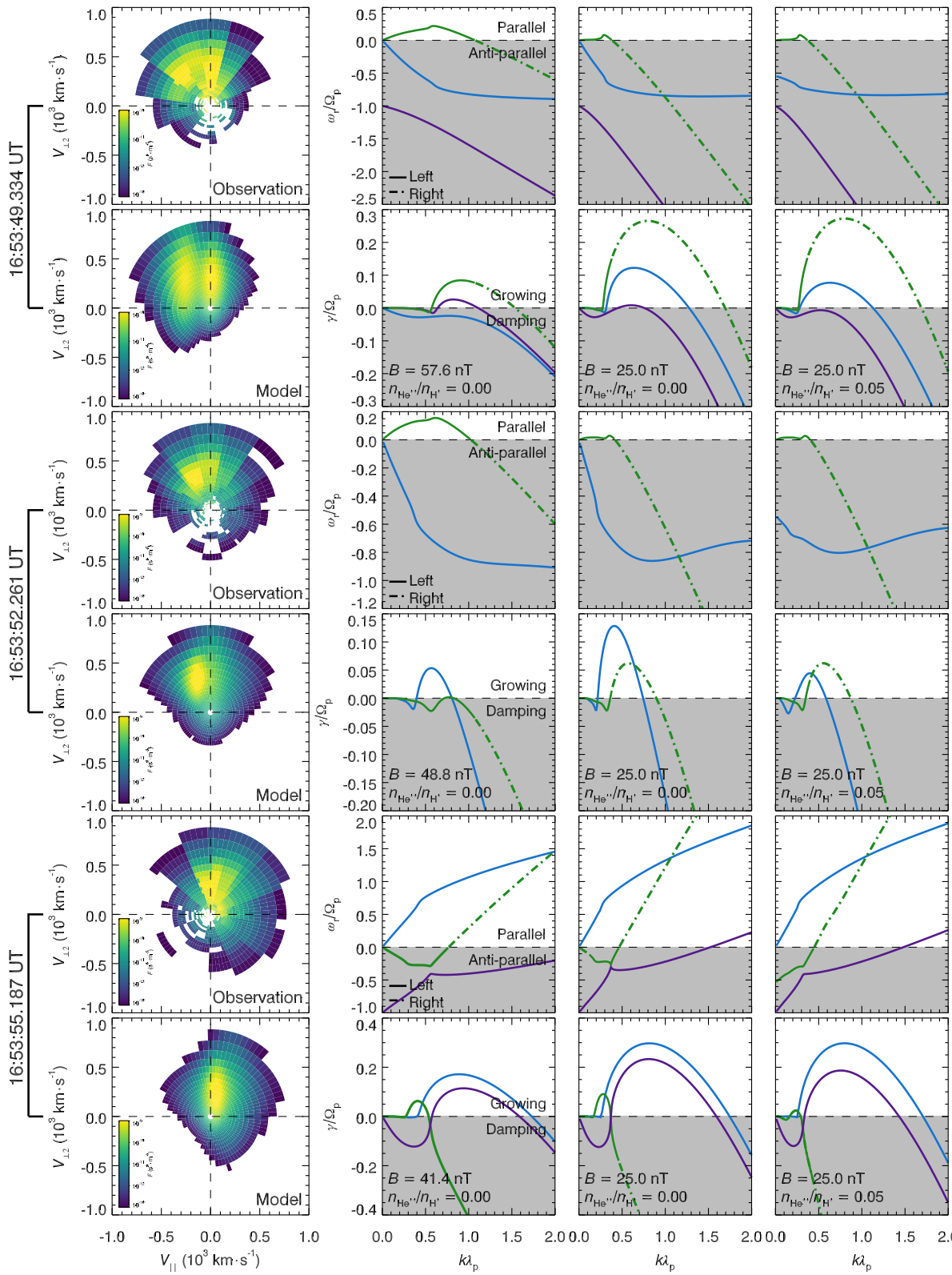

Figure 3.

Information S1, using a superposition of multiple κ-Maxwellian distributions, we fit the observed proton distributions from 16:53:49 UT to 16:55:29 UT. From the magnetosheath to the boundary layer, both the parallel and perpendicular temperatures tended to increase, with the perpendicular temperature exhibiting a more significant increase. The boundary layer observed here showed no significant decrease in plasma density or increase in magnetic field strength (Figure S6 in Supporting Information S1), different from the plasma depletion layer with the adiabatic heating of ions (Anderson et al., 1991; Hasegawa, 2012; Zwan & Wolf, 1976). These observations suggest that this magnetopause reconnection produced perpendicular-preferential heating of protons.

Our findings appear to contrast with previous observational, theoretical, and numerical studies. Phan et al. (2014) introduced the proton "bulk temperature" as the second moment of the proton distributions. Their statistical survey indicated that during magnetopause reconnection, regardless of the shear angle, the parallel and perpendicular temperature increments are $\Delta T_{\parallel} = 0.2 m_i V_A^2$ and $\Delta T_{\perp} = 0.1 m_i V_A^2$, respectively. In our analysis, we utilized two or three components with different parallel drift velocities but identical perpendicular drift velocities. Consequently, the obtained parallel thermodynamic temperature is expected to be lower than the corresponding parallel bulk temperature, while the perpendicular thermodynamic temperature should closely match the perpendicular bulk temperature. Our next focus will be on analyzing the characteristics of the first (and most significant) component derived from fitting. The observed increase in parallel temperature was $\Delta T_{\parallel} = 0.03 - 0.06\ m_i V_A^2$, which is 3–6 times smaller than the values reported by Phan et al. (2014). This discrepancy may be partially attributed to differences in the definition of temperature. Conversely, the increase in perpendicular temperature was $\Delta T_{\perp} = 0.09 - 0.40\ m_i V_A^2$, with the maximum value being up to four times greater than the statistically averaged values (Phan et al., 2014). Notably, the observed perpendicular temperature of protons showed no positive correlation with magnetic field strength (see Figure S6 in Supporting Information S1), thereby ruling out the adiabatic betatron heating mechanism (Eastwood et al., 2015; Lu et al., 2016). Drake, Cassak, et al. (2009) proposed the "pickup" mechanism for the nonadiabatic perpendicular heating of ions under strong guide fields. However, protons with a low mass-to-charge ratio generally do not satisfy the criteria for pickup heating (Drake, Cassak, et al., 2009; Drake & Swisdak, 2014). Moreover, the ring distributions predicted by the pickup heating scenario were unobservable. Observations and simulations of magnetotail reconnection (Eastwood et al., 2015; Hietala et al., 2015) suggested that the Speiser-like motion of ions contributes to the increase in perpendicular temperature, leading to ion distributions forming crescent or horseshoe shapes. Unlike symmetric magnetotail reconnection, magnetopause reconnection is asymmetric and occurs in a lower plasma beta environment. The expected ion distributions related to Speiser-like motions were also not observed in our event. Thus, how protons are preferentially heated perpendicularly during magnetopause reconnection remains an open question.

6. Summary

We present the first observation of EMIC waves within the magnetic reconnection exhaust at Earth's magnetopause. The detected EMIC waves exhibited two distinct spectral signatures: (a) a rising-tone emission with right-handed polarization and (b) a falling-tone emission with left-handed polarization. Our calculations based on linear instability theory indicate that cyclotron instability driven by temperature-anisotropic proton beams was responsible for generating these EMIC waves. The chirping-frequency wave packet likely involved nonlinear amplification processes similar to those documented in the inner magnetosphere (An et al., 2024; Omura et al., 2010). Our measurements reveal a consistent trend from the magnetosheath through the boundary layer (including the embedded reconnection exhaust): both parallel and perpendicular proton temperatures increased, with the perpendicular-to-parallel temperature anisotropy becoming more pronounced. These results demonstrate that magnetopause reconnection caused perpendicular-preferential heating of protons, contrasting with prior theoretical, observational, and numerical predictions of parallel-preferential proton heating. Our finding calls for

Figure 3. Linear instability analysis of anisotropic proton beams at three adjacent time moments (16:53:49 UT, 16:53:52 UT, and 16:53:55 UT) in the magnetic reconnection exhaust. Column 1 compares observed and modeled ion velocity distributions (color-coded) in the MFA coordinate system. Columns 2–4 present instability tests for parallel and anti-parallel propagating waves, with each panel pair showing dispersion relations (upper) and growth rates (lower). Color-coding distinguishes dispersion branches, while solid and dashed curves indicate left- and right-handed polarizations respectively. Frequency signs denote propagation direction (positive for parallel and negative for anti-parallel). Growth rate panels specify test parameters such as magnetic field strength and He^{++} abundance. The wave angular frequency ω and wavenumber k are normalized by the proton gyrofrequency Ω_p and inertial length λ_p, respectively.

revised theoretical frameworks to reconcile the observed perpendicular-preferential heating with established reconnection paradigms.

Conflict of Interest

The authors declare no conflicts of interest relevant to this study.

Data Availability Statement

BO-KM code is available at github website (Bai & Xie, 2025). THEMIS data are available at THEMIS mission homepage (2025). Specifically, we have analyzed the following data: ESA L0 data (2025), ESA L2 data (Angelopoulos, Carlson, & McFadden, 2025), FGM L2 data (2025), and EFI L2 data (Angelopoulos, Bonnell, & Mozer, 2025). The He^{++}/H^{+} density ratio in the upstream solar wind is taken from Papitashvili and King (2025).

Acknowledgments
We acknowledge the entire THEMIS team for the use of data. This work was supported by the National Natural Science Foundation of China Grants 42188101, 42441808, 42130204, 42274198, 42422406, and 42174185, the Postdoctoral Fellowship Program of China Postdoctoral Science Foundation GZB20240701 and the open project fund of State Key Laboratory of Lunar and Planetary Sciences No. 002/2024/SKL.

References

An, Z., Tao, X., Zonca, F., & Chen, L. (2024). Frequency chirping of electromagnetic ion cyclotron waves in Earth's magnetosphere. *Geophysical Research Letters*, *51*(4), e2023GL106456. https://doi.org/10.1029/2023GL106456

Anderson, B. J., Fuselier, S. A., Gary, S. P., & Denton, R. E. (1994). Magnetic spectral signatures in the Earth's magnetosheath and plasma depletion layer. *Journal of Geophysical Research*, *99*(A4), 5877–5892. https://doi.org/10.1029/93JA02827

Anderson, B. J., Fuselier, S. A., & Murr, D. (1991). Electromagnetic ion cyclotron waves observed in the plasma depletion layer. *Geophysical Research Letters*, *18*(11), 1955–1958. https://doi.org/10.1029/91GL02238

Angelopoulos, V. (2008). The THEMIS mission. *Space Science Reviews*, *141*(1–4), 5–34. https://doi.org/10.1007/s11214-008-9336-1

Angelopoulos, V., Bonnell, J. W., & Mozer, F. S. (2025). THEMIS-A (P5), electric field instrument (EFI) spacecraft measured electric field [Dataset]. Retrieved from https://themis.ssl.berkeley.edu/data/themis/tha/l2/efi/.NASASpacePhysicsDataFacility

Angelopoulos, V., Carlson, C. W., & McFadden, J. P. (2025). THEMIS-A: ESA electron/ion energy fluxes and moments [Dataset]. *NASA Space Physics Data Facility*. Retrieved from https://themis.ssl.berkeley.edu/data/themis/tha/l2/esa/

Auster, H. U., Glassmeier, K. H., Magnes, W., Aydogar, O., Baumjohann, W., Constantinescu, D., et al. (2008). The THEMIS fluxgate magnetometer. *Space Science Reviews*, *141*(1–4), 235–264. https://doi.org/10.1007/s11214-008-9365-9

Bai, W., & Xie, H. (2025). BO-KM code [Software]. Retrieved from https://github.com/baiweiphys/BO-KM/

Bai, W., Xie, H., Wu, C., Pu, Y., & Yu, P. (2025). BO-KM: A comprehensive solver for dispersion relation of obliquely propagating waves in magnetized multi-species plasma with anisotropic drift kappa-Maxwellian distribution. *Computer Physics Communications*, *307*, 109434. https://doi.org/10.1016/j.cpc.2024.109434

Bale, S. D., Mozer, F. S., & Phan, T. (2002). Observation of lower hybrid drift instability in the diffusion region at a reconnecting magnetopause. *Geophysical Research Letters*, *29*(24), 2180. https://doi.org/10.1029/2002GL016113

Bastian, T. S., Benz, A. O., & Gary, D. E. (1998). Radio emission from solar flares. *Annual Review of Astronomy and Astrophysics*, *36*(1), 131–188. https://doi.org/10.1146/annurev.astro.36.1.131

Bonnell, J. W., Mozer, F. S., Delory, G. T., Hull, A. J., Ergun, R. E., Cully, C. M., et al. (2008). The electric field instrument (EFI) for THEMIS. *Space Science Reviews*, *141*(1–4), 303–341. https://doi.org/10.1007/s11214-008-9469-2

Burch, J. L., Dokgo, K., Hwang, K. J., Torbert, R. B., Graham, D. B., Webster, J. M., et al. (2019). High-frequency wave generation in magnetotail reconnection: Linear dispersion analysis. *Geophysical Research Letters*, *46*(8), 4089–4097. https://doi.org/10.1029/2019GL082471

Burch, J. L., Torbert, R. B., Phan, T. D., Chen, L. J., Moore, T. E., Ergun, R. E., et al. (2016). Electron-scale measurements of magnetic reconnection in space. *Science*, *352*(6290), aaf2939. https://doi.org/10.1126/science.aaf2939

Cassak, P. A., & Shay, M. A. (2007). Scaling of asymmetric magnetic reconnection: General theory and collisional simulations. *Physics of Plasmas*, *14*(10), 102114. https://doi.org/10.1063/1.2795630

Cattell, C., Dombeck, J., Wygant, J., Drake, J. F., Swisdak, M., Goldstein, M. L., et al. (2005). Cluster observations of electron holes in association with magnetotail reconnection and comparison to simulations. *Journal of Geophysical Research*, *110*(A1), A01211. https://doi.org/10.1029/2004JA010519

Chang, C., Huang, K., Lu, Q., Lu, S., Yu, X., Wang, R., et al. (2022). Electrostatic solitary waves and electron-beam instabilities in the separatrix region of magnetic reconnection. *The Astrophysical Journal*, *933*(1), 67. https://doi.org/10.3847/1538-4357/ac738d

Chang, C., Huang, K., Lu, Q., Sang, L., Lu, S., Wang, R., et al. (2021). Particle-in-cell simulations of electrostatic solitary waves in asymmetric magnetic reconnection. *Journal of Geophysical Research: Space Physics*, *126*(7), e29290. https://doi.org/10.1029/2021JA029290

Dai, L. (2009). Collisionless magnetic reconnection via Alfvén eigenmodes. *Physical Review Letters*, *102*(24), 245003. https://doi.org/10.1103/PhysRevLett.102.245003

Dai, L., Wang, C., Zhang, Y., Lavraud, B., Burch, J., Pollock, C., & Torbert, R. B. (2017). Kinetic Alfvén wave explanation of the Hall fields in magnetic reconnection. *Geophysical Research Letters*, *44*(2), 634–640. https://doi.org/10.1002/2016GL071044

Dai, L., Zhu, M., Ren, Y., Gonzalez, W., Wang, C., Sibeck, D., et al. (2024). Global-scale magnetosphere convection driven by dayside magnetic reconnection. *Nature Communications*, *15*(1), 639. https://doi.org/10.1038/s41467-024-44992-y

Daughton, W. (2003). Electromagnetic properties of the lower-hybrid drift instability in a thin current sheet. *Physics of Plasmas*, *10*(8), 3103–3119. https://doi.org/10.1063/1.1594724

Davidson, R. C., & Ogden, J. M. (1975). Electromagnetic ion cyclotron instability driven by ion energy anisotropy in high-beta plasmas. *Physics of Fluids*, *18*(8), 1045–1050. https://doi.org/10.1063/1.861253

Deng, X. H., & Matsumoto, H. (2001). Rapid magnetic reconnection in the Earth's magnetosphere mediated by whistler waves. *Nature*, *410*(6828), 557–560. https://doi.org/10.1038/35069018

Deng, X. H., Matsumoto, H., Kojima, H., Mukai, T., Anderson, R. R., Baumjohann, W., & Nakamura, R. (2004). Geotail encounter with reconnection diffusion region in the Earth's magnetotail: Evidence of multiple X lines collisionless reconnection? *Journal of Geophysical Research*, *109*(A5), A05206. https://doi.org/10.1029/2003JA010031

Denton, R. E., Gary, S. P., Anderson, B. J., Fuselier, S. A., & Hudson, M. K. (1994). Low-frequency magnetic fluctuation spectra in the magnetosheath and plasma depletion layer. *Journal of Geophysical Research*, *99*(A4), 5893–5902. https://doi.org/10.1029/93JA02729

Divin, A., Khotyaintsev, Y. V., Vaivads, A., & André, M. (2015). Lower hybrid drift instability at a dipolarization front. *Journal of Geophysical Research: Space Physics*, *120*(2), 1124–1132. https://doi.org/10.1002/2014JA020528

Divin, A., Khotyaintsev, Y. V., Vaivads, A., André, M., Markidis, S., & Lapenta, G. (2015). Evolution of the lower hybrid drift instability at reconnection jet front. *Journal of Geophysical Research: Space Physics*, *120*(4), 2675–2690. https://doi.org/10.1002/2014JA020503

Drake, J. F., Cassak, P. A., Shay, M. A., Swisdak, M., & Quataert, E. (2009). A magnetic reconnection mechanism for ion acceleration and abundance enhancements in impulsive flares. *The Astrophysical Journal Letters*, *700*(1), L16–L20. https://doi.org/10.1088/0004-637X/700/1/L16

Drake, J. F., & Swisdak, M. (2014). The onset of ion heating during magnetic reconnection with a strong guide field. *Physics of Plasmas*, *21*(7), 072903. https://doi.org/10.1063/1.4889871

Drake, J. F., Swisdak, M., Cattell, C., Shay, M. A., Rogers, B. N., & Zeiler, A. (2003). Formation of electron holes and particle energization during magnetic reconnection. *Science*, *299*(5608), 873–877. https://doi.org/10.1126/science.1080333

Drake, J. F., Swisdak, M., Phan, T. D., Cassak, P. A., Shay, M. A., Lepri, S. T., et al. (2009). Ion heating resulting from pickup in magnetic reconnection exhausts. *Journal of Geophysical Research*, *114*(A5), A05111. https://doi.org/10.1029/2008JA013701

Duan, S., Dai, L., Wang, C., He, Z., Cai, C., Zhang, Y. C., et al. (2017). Oxygen ions O^+ energized by kinetic Alfvén eigenmode during dipolarizations of intense substorms. *Journal of Geophysical Research: Space Physics*, *122*(11), 11256–11273. https://doi.org/10.1002/2017JA024418

Eastwood, J. P., Goldman, M. V., Hietala, H., Newman, D. L., Mistry, R., & Lapenta, G. (2015). Ion reflection and acceleration near magnetotail dipolarization fronts associated with magnetic reconnection. *Journal of Geophysical Research: Space Physics*, *120*(1), 511–525. https://doi.org/10.1002/2014JA020516

ESA L0 data. (2025). The Electrostatic Analyzers (ESA) Level 0 data [Dataset]. Retrieved from https://themis.ssl.berkeley.edu/data/themis/tha/l0/

Farrell, W. M., Desch, M. D., Kaiser, M. L., & Goetz, K. (2002). The dominance of electron plasma waves near a reconnection X-line region. *Geophysical Research Letters*, *29*(19), 1902. https://doi.org/10.1029/2002GL014662

FGM L2 data. (2025). The Fluxgate Magnetometer (FGM) Level 2 data [Dataset]. Retrieved from https://themis.ssl.berkeley.edu/data/themis/tha/l2/fgm/

Fu, H. S., Cao, J. B., Cully, C. M., Khotyaintsev, Y. V., Vaivads, A., Angelopoulos, V., et al. (2014). Whistler-mode waves inside flux pileup region: Structured or unstructured? *Journal of Geophysical Research: Space Physics*, *119*(11), 9089–9100. https://doi.org/10.1002/2014JA020204

Fu, H. S., Peng, F. Z., Liu, C. M., Burch, J. L., Gershman, D. G., & Le Contel, O. (2019). Evidence of electron acceleration at a reconnecting magnetopause. *Geophysical Research Letters*, *46*(11), 5645–5652. https://doi.org/10.1029/2019GL083032

Fujimoto, K. (2014). Wave activities in separatrix regions of magnetic reconnection. *Geophysical Research Letters*, *41*(8), 2721–2728. https://doi.org/10.1002/2014GL059893

Fujimoto, K., & Machida, S. (2006). A generation mechanism of electrostatic waves and subsequent electron heating in the plasma sheet-lobe boundary region during magnetic reconnection. *Journal of Geophysical Research*, *111*(A9), A09216. https://doi.org/10.1029/2005JA011542

Fujimoto, K., & Sydora, R. D. (2008). Whistler waves associated with magnetic reconnection. *Geophysical Research Letters*, *35*(19), L19112. https://doi.org/10.1029/2008GL035201

Fujimoto, K., & Sydora, R. D. (2012). Plasmoid-induced turbulence in collisionless magnetic reconnection. *Physical Review Letters*, *109*(26), 265004. https://doi.org/10.1103/PhysRevLett.109.265004

Fujimoto, M., Shinohara, I., & Kojima, H. (2011). Reconnection and waves: A review with a perspective. *Space Science Reviews*, *160*(1–4), 123–143. https://doi.org/10.1007/s11214-011-9807-7

Gary, S. P. (1991). Electromagnetic ion/ion instabilities and their consequences in space plasmas: A review. *Space Science Reviews*, *56*(3–4), 373–415. https://doi.org/10.1007/BF00196632

Gary, S. P. (1992). The mirror and ion cyclotron anisotropy instabilities. *Journal of Geophysical Research*, *97*(A6), 8519–8529. https://doi.org/10.1029/92JA00299

Gary, S. P., Fuselier, S. A., & Anderson, B. J. (1993). Ion anisotropy instabilities in the magnetosheath. *Journal of Geophysical Research*, *98*(A2), 1481–1488. https://doi.org/10.1029/92JA01844

Goldman, M. V., Newman, D. L., Lapenta, G., Andersson, L., Gosling, J. T., Eriksson, S., et al. (2014). Čerenkov emission of quasiparallel whistlers by fast electron phase-space holes during magnetic reconnection. *Physical Review Letters*, *112*(14), 145002. https://doi.org/10.1103/PhysRevLett.112.145002

Gosling, J. T., Thomsen, M. F., Bame, S. J., Elphic, R. C., & Russell, C. T. (1990). Plasma flow reversals at the dayside magnetopause and the origin of asymmetric polar cap convection. *Journal of Geophysical Research*, *95*(A6), 8073–8084. https://doi.org/10.1029/JA095iA06p08073

Graham, D. B., Khotyaintsev, Y. V., Norgren, C., Vaivads, A., André, M., Drake, J. F., et al. (2019). Universality of lower hybrid waves at Earth's magnetopause. *Journal of Geophysical Research: Space Physics*, *124*(11), 8727–8760. https://doi.org/10.1029/2019JA027155

Graham, D. B., Khotyaintsev, Y. V., Vaivads, A., Norgren, C., André, M., Webster, J. M., et al. (2017). Instability of agyrotropic electron beams near the electron diffusion region. *Physical Review Letters*, *119*(2), 025101. https://doi.org/10.1103/PhysRevLett.119.025101

Graham, D. B., Vaivads, A., Khotyaintsev, Y. V., André, M., Le Contel, O., Malaspina, D. M., et al. (2018). Large-amplitude high-frequency waves at Earth's magnetopause. *Journal of Geophysical Research: Space Physics*, *123*(4), 2630–2657. https://doi.org/10.1002/2017JA025034

Grison, B., Hanzelka, M., Breuillard, H., Darrouzet, F., Santolík, O., Cornilleau-Wehrlin, N., & Dandouras, I. (2018). Plasmaspheric plumes and EMIC rising tone emissions. *Journal of Geophysical Research: Space Physics*, *123*(11), 9443–9452. https://doi.org/10.1029/2018JA025796

Hasegawa, H. (2012). Structure and dynamics of the magnetopause and its boundary layers. *Monographs on Environment, Earth and Planets*, *1*(2), 71–119. https://doi.org/10.5047/meep.2012.00102.0071

Hellberg, M. A., & Mace, R. L. (2002). Generalized plasma dispersion function for a plasma with a kappa-Maxwellian velocity distribution. *Physics of Plasmas*, *9*(5), 1495–1504. https://doi.org/10.1063/1.1462636

Hietala, H., Drake, J. F., Phan, T. D., Eastwood, J. P., & McFadden, J. P. (2015). Ion temperature anisotropy across a magnetotail reconnection jet. *Geophysical Research Letters*, *42*(18), 7239–7247. https://doi.org/10.1002/2015GL065168

Horne, R. B., & Miyoshi, Y. (2016). Propagation and linear mode conversion of magnetosonic and electromagnetic ion cyclotron waves in the radiation belts. *Geophysical Research Letters*, *43*(19), 10034–10039. https://doi.org/10.1002/2016GL070216

Horne, R. B., & Thorne, R. M. (1993). On the preferred source location for the convective amplification of ion cyclotron waves. *Journal of Geophysical Research*, *98*(A6), 9233–9248. https://doi.org/10.1029/92JA02972

Hoshino, M., Saito, Y., Mukai, T., Nishida, A., Kokubun, S., & Yamamoto, T. (1997). Origin of hot and high speed plasmas in plasma sheet: Plasma acceleration and heating due to slow shocks. *Advances in Space Research*, *20*(4–5), 973–982. https://doi.org/10.1016/S0273-1177(97)00505-X

Huang, S. Y., Fu, H. S., Yuan, Z. G., Vaivads, A., Khotyaintsev, Y. V., Retino, A., et al. (2016). Two types of whistler waves in the hall reconnection region. *Journal of Geophysical Research: Space Physics*, *121*(7), 6639–6646. https://doi.org/10.1002/2016JA022650

Huang, S. Y., Zhou, M., Sahraoui, F., Deng, X. H., Pang, Y., Yuan, Z. G., et al. (2010). Wave properties in the magnetic reconnection diffusion region with high β: Application of the k-filtering method to Cluster multispacecraft data. *Journal of Geophysical Research*, *115*(A12), A12211. https://doi.org/10.1029/2010JA015335

Keika, K., Spasojevic, M., Li, W., Bortnik, J., Miyoshi, Y., & Angelopoulos, V. (2012). PENGUIn/AGO and THEMIS conjugate observations of whistler mode chorus waves in the dayside uniform zone under steady solar wind and quiet geomagnetic conditions. *Journal of Geophysical Research*, *117*(A7), A07212. https://doi.org/10.1029/2012JA017708

Khotyaintsev, Y. V., Cully, C. M., Vaivads, A., André, M., & Owen, C. J. (2011). Plasma jet braking: Energy dissipation and nonadiabatic electrons. *Physical Review Letters*, *106*(16), 165001. https://doi.org/10.1103/PhysRevLett.106.165001

Khotyaintsev, Y. V., Graham, D. B., Norgren, C., & Vaivads, A. (2019). Collisionless magnetic reconnection and waves: Progress review. *Frontiers in Astronomy and Space Sciences*, *6*, 70. https://doi.org/10.3389/fspas.2019.00070

Lapenta, G., Markidis, S., Divin, A., Goldman, M. V., & Newman, D. L. (2011). Bipolar electric field signatures of reconnection separatrices for a hydrogen plasma at realistic guide fields. *Geophysical Research Letters*, *38*(17), L17104. https://doi.org/10.1029/2011GL048572

Lee, L. C., & Lee, K. H. (2020). Fluid and kinetic aspects of magnetic reconnection and some related magnetospheric phenomena. *Reviews of Modern Plasma Physics*, *4*(1), 9. https://doi.org/10.1007/s41614-020-00045-7

Li, W. Y., Graham, D. B., Khotyaintsev, Y. V., Vaivads, A., André, M., Min, K., et al. (2020). Electron Bernstein waves driven by electron crescents near the electron diffusion region. *Nature Communications*, *11*(1), 141. https://doi.org/10.1038/s41467-019-13920-w

Lu, S., Angelopoulos, V., & Fu, H. (2016). Suprathermal particle energization in dipolarization fronts: Particle-in-cell simulations. *Journal of Geophysical Research: Space Physics*, *121*(10), 9483–9500. https://doi.org/10.1002/2016JA022815

Matsumoto, H., Deng, X. H., Kojima, H., & Anderson, R. R. (2003). Observation of electrostatic solitary waves associated with reconnection on the dayside magnetopause boundary. *Geophysical Research Letters*, *30*(6), 1326. https://doi.org/10.1029/2002GL016319

McCollough, J. P., Elkington, S. R., Usanova, M. E., Mann, I. R., Baker, D. N., & Kale, Z. C. (2010). Physical mechanisms of compressional EMIC wave growth. *Journal of Geophysical Research*, *115*(A10), A10214. https://doi.org/10.1029/2010JA015393

McFadden, J. P., Carlson, C. W., Larson, D., Ludlam, M., Abiad, R., Elliott, B., et al. (2008). The THEMIS ESA plasma instrument and in-flight calibration. *Space Science Reviews*, *141*(1–4), 277–302. https://doi.org/10.1007/s11214-008-9440-2

Mozer, F. S., Agapitov, O. V., Giles, B., & Vasko, I. (2018). Direct observation of electron distributions inside millisecond duration electron holes. *Physical Review Letters*, *121*(13), 135102. https://doi.org/10.1103/PhysRevLett.121.135102

Nakamura, S., Omura, Y., & Angelopoulos, V. (2016). A statistical study of EMIC rising and falling tone emissions observed by THEMIS. *Journal of Geophysical Research: Space Physics*, *121*(9), 8374–8391. https://doi.org/10.1002/2016JA022353

Omura, Y., Katoh, Y., & Summers, D. (2008). Theory and simulation of the generation of whistler-mode chorus. *Journal of Geophysical Research*, *113*(A4), A04223. https://doi.org/10.1029/2007JA012622

Omura, Y., Nakamura, S., Kletzing, C. A., Summers, D., & Hikishima, M. (2015). Nonlinear wave growth theory of coherent hiss emissions in the plasmasphere. *Journal of Geophysical Research: Space Physics*, *120*(9), 7642–7657. https://doi.org/10.1002/2015JA021520

Omura, Y., Pickett, J., Grison, B., Santolik, O., Dandouras, I., Engebretson, M., et al. (2010). Theory and observation of electromagnetic ion cyclotron triggered emissions in the magnetosphere. *Journal of Geophysical Research*, *115*(A7), A07234. https://doi.org/10.1029/2010JA015300

Papitashvili, N. E., & King, J. H. (2025). OMNI hourly data set [Dataset]. Retrieved from https://cdaweb.gsfc.nasa.gov/.NASASpacePhysicsDataFacility

Parker, E. N. (1957). Sweet's mechanism for merging magnetic fields in conducting fluids. *Journal of Geophysical Research*, *62*(4), 509–520. https://doi.org/10.1029/JZ062i004p00509

Paschmann, G., Papamastorakis, I., Sckopke, N., Haerendel, G., Sonnerup, B. U. O., Bame, S. J., et al. (1979). Plasma acceleration at the Earth's magnetopause—Evidence for reconnection. *Nature*, *282*(5736), 243–246. https://doi.org/10.1038/282243a0

Phan, T. D., Drake, J. F., Shay, M. A., Gosling, J. T., Paschmann, G., Eastwood, J. P., et al. (2014). Ion bulk heating in magnetic reconnection exhausts at Earth's magnetopause: Dependence on the inflow Alfvén speed and magnetic shear angle. *Geophysical Research Letters*, *41*(20), 7002–7010. https://doi.org/10.1002/2014GL061547

Pickett, J. S., Grison, B., Omura, Y., Engebretson, M. J., Dandouras, I., Masson, A., et al. (2010). Cluster observations of EMIC triggered emissions in association with Pc1 waves near Earth's plasmapause. *Geophysical Research Letters*, *37*(9), L09104. https://doi.org/10.1029/2010GL042648

Pritchett, P. L., & Coroniti, F. V. (2004). Three-dimensional collisionless magnetic reconnection in the presence of a guide field. *Journal of Geophysical Research*, *109*(A1), A01220. https://doi.org/10.1029/2003JA009999

Remya, B., Tsurutani, B. T., Reddy, R. V., Lakhina, G. S., Falkowski, B. J., Echer, E., & Glassmeier, K. H. (2014). Large-amplitude, circularly polarized, compressive, obliquely propagating electromagnetic proton cyclotron waves throughout the Earth's magnetosheath: Low plasma β conditions. *The Astrophysical Journal*, *793*(1), 6. https://doi.org/10.1088/0004-637X/793/1/6

Ren, Y., Dai, L., Li, W., Tao, X., Wang, C., Tang, B., et al. (2019). Whistler waves driven by field-aligned streaming electrons in the near-Earth magnetotail reconnection. *Geophysical Research Letters*, *46*(10), 5045–5054. https://doi.org/10.1029/2019GL083283

Ren, Y., Dai, L., Wang, C., & Guo, Z. (2023). The wave growth, saturation, and electron heating of lower hybrid waves in the magnetic reconnection exhaust. *The Astrophysical Journal*, *956*(2), 143. https://doi.org/10.3847/1538-4357/acf855

Ren, Y., Dai, L., Wang, C., & Lavraud, B. (2022). Parallel electron heating through Landau resonance with lower hybrid waves at the edge of reconnection ion jets. *The Astrophysical Journal*, *928*(1), 5. https://doi.org/10.3847/1538-4357/ac53fb

Ren, Y., Dai, L., Wang, C., & Lavraud, B. (2023). Statistical properties of lower hybrid waves in the magnetopause reconnection exhaust region. *Journal of Geophysical Research: Space Physics*, *128*(3), e2022JA031242. https://doi.org/10.1029/2022JA031242

Ren, Y., Dai, L., Wang, C., Lavraud, B., Escoubet, C. P., & Burch, J. L. (2024). Capsule electron distributions near the diffusion region of magnetic reconnection. *Geophysical Research Letters*, *51*(23), 2024GL112074. https://doi.org/10.1029/2024GL112074

Retinò, A., Vaivads, A., André, M., Sahraoui, F., Khotyaintsev, Y., Pickett, J. S., et al. (2006). Structure of the separatrix region close to a magnetic reconnection X-line: Cluster observations. *Geophysical Research Letters*, *33*(6), L06101. https://doi.org/10.1029/2005GL024650

Rogers, B. N., Denton, R. E., Drake, J. F., & Shay, M. A. (2001). Role of dispersive waves in collisionless magnetic reconnection. *Physical Review Letters*, *87*(19), 195004. https://doi.org/10.1103/PhysRevLett.87.195004

Roytershteyn, V., Daughton, W., Karimabadi, H., & Mozer, F. S. (2012). Influence of the lower-hybrid drift instability on magnetic reconnection in asymmetric configurations. *Physical Review Letters*, *108*(18), 185001. https://doi.org/10.1103/PhysRevLett.108.185001

Roytershteyn, V., Dorfman, S., Daughton, W., Ji, H., Yamada, M., & Karimabadi, H. (2013). Electromagnetic instability of thin reconnection layers: Comparison of three-dimensional simulations with MRX observations. *Physics of Plasmas*, *20*(6), 061212. https://doi.org/10.1063/1.4811371

Sakai, J. I., Kitamoto, T., & Saito, S. (2005). Simulation of solar type III radio bursts from a magnetic reconnection region. *The Astrophysical Journal*, *622*(2), L157–L160. https://doi.org/10.1086/429665

Santolík, O., Parrot, M., & Lefeuvre, F. (2003). Singular value decomposition methods for wave propagation analysis. *Radio Science*, *38*(1), 1010. https://doi.org/10.1029/2000RS002523

Santolík, O., Pickett, J. S., Gurnett, D. A., Menietti, J. D., Tsurutani, B. T., & Verkhoglyadova, O. (2010). Survey of Poynting flux of whistler mode chorus in the outer zone. *Journal of Geophysical Research*, *115*(15), A00F13. https://doi.org/10.1029/2009JA014925

Santolík, O., Pickett, J. S., Gurnett, D. A., & Storey, L. R. O. (2002). Magnetic component of narrowband ion cyclotron waves in the auroral zone. *Journal of Geophysical Research*, *107*(A12), 1444. https://doi.org/10.1029/2001JA000146

Sonnerup, B. U. O., & Cahill, L. J., Jr. (1967). Magnetopause structure and attitude from explorer 12 observations. *Journal of Geophysical Research*, *72*(1), 171. https://doi.org/10.1029/JZ072i001p00171

Sugiyama, H., Singh, S., Omura, Y., Shoji, M., Nunn, D., & Summers, D. (2015). Electromagnetic ion cyclotron waves in the Earth's magnetosphere with a kappa-Maxwellian particle distribution. *Journal of Geophysical Research: Space Physics*, *120*(10), 8426–8439. https://doi.org/10.1002/2015JA021346

Tang, B. B., Li, W. Y., Graham, D. B., Rager, A. C., Wang, C., Khotyaintsev, Y. V., et al. (2019). Crescent-shaped electron distributions at the nonreconnecting magnetopause: Magnetospheric multiscale observations. *Geophysical Research Letters*, *46*(6), 3024–3032. https://doi.org/10.1029/2019GL082231

Tang, X., Cattell, C., Dombeck, J., Dai, L., Wilson, L. B., Breneman, A., & Hupach, A. (2013). THEMIS observations of the magnetopause electron diffusion region: Large amplitude waves and heated electrons. *Geophysical Research Letters*, *40*(12), 2884–2890. https://doi.org/10.1002/grl.50565

Tao, X., Zonca, F., & Chen, L. (2021). A "Trap-Release-Amplify" model of chorus waves. *Journal of Geophysical Research: Space Physics*, *126*(9), e29585. https://doi.org/10.1029/2021JA029585

THEMIS mission homepage. (2025). Time history of events and macroscale interactions during substorms (THEMIS) data [Dataset]. Retrieved from https://themis.ssl.berkeley.edu/data/themis/

Tsyganenko, N. A., & Sitnov, M. I. (2005). Modeling the dynamics of the inner magnetosphere during strong geomagnetic storms. *Journal of Geophysical Research*, *110*(A3), A03208. https://doi.org/10.1029/2004JA010798

Vaivads, A., Khotyaintsev, Y., André, M., & Treumann, R. A. (2006). Plasma waves near reconnection sites. In J. W. Labelle & R. A. Treumann (Eds.), *Geospace electromagnetic waves and radiation* (Vol. 687, pp. 251–269). https://doi.org/10.1007/3-540-33203-0_10

Vines, S. K., Allen, R. C., Anderson, B. J., Engebretson, M. J., Fuselier, S. A., Russell, C. T., et al. (2019). EMIC waves in the outer magnetosphere: Observations of an off-equator source region. *Geophysical Research Letters*, *46*(11), 5707–5716. https://doi.org/10.1029/2019GL082152

Walsh, B. M., Foster, J. C., Erickson, P. J., & Sibeck, D. G. (2014). Simultaneous ground- and space-based observations of the plasmaspheric plume and reconnection. *Science*, *343*(6175), 1122–1125. https://doi.org/10.1126/science.1247212

Wang, R., Wang, S., Lu, Q., Li, X., Lu, S., & Gonzalez, W. (2023). Direct observation of turbulent magnetic reconnection in the solar wind. *Nature Astronomy*, *7*(1), 18–28. https://doi.org/10.1038/s41550-022-01818-5

Wu, M., Volwerk, M., Lu, Q., VöRöS, Z., Nakamura, R., & Zhang, T. (2013). The proton temperature anisotropy associated with bursty bulk flows in the magnetotail. *Journal of Geophysical Research: Space Physics*, *118*(8), 4875–4883. https://doi.org/10.1002/jgra.50451

Xie, H.-S. (2019). BO: A unified tool for plasma waves and instabilities analysis. *Computer Physics Communications*, *244*, 343–371. https://doi.org/10.1016/j.cpc.2019.06.014

Yu, X., Lu, Q., Wang, R., Huang, K., Gao, X., & Wang, S. (2021). MMS observations of broadband electrostatic waves in electron diffusion region of magnetotail reconnection. *Journal of Geophysical Research: Space Physics*, *126*(3), e28882. https://doi.org/10.1029/2020JA028882

Zhao, J. S., Wang, T. Y., Dunlop, M. W., Shi, C., He, J. S., Dong, X. C., et al. (2019). Large-amplitude electromagnetic ion cyclotron waves and density fluctuations in the flank of the Earth's magnetosheath. *Geophysical Research Letters*, *46*(9), 4545–4553. https://doi.org/10.1029/2019GL081964

Zhou, M., Ashour-Abdalla, M., Deng, X., Schriver, D., El-Alaoui, M., & Pang, Y. (2009). THEMIS observation of multiple dipolarization fronts and associated wave characteristics in the near-Earth magnetotail. *Geophysical Research Letters*, *36*(20), L20107. https://doi.org/10.1029/2009GL040663

Zhou, M., Zhong, Z., & Deng, X. (2022). Kinetic properties of collisionless magnetic reconnection in space plasma: In situ observations. *Reviews of Modern Plasma Physics*, *6*(1), 15. https://doi.org/10.1007/s41614-022-00079-z

Zwan, B. J., & Wolf, R. A. (1976). Depletion of solar wind plasma near a planetary boundary. *Journal of Geophysical Research*, *81*(10), 1636–1648. https://doi.org/10.1029/JA081i010p01636